

Molecular gas, CO, and star formation in galaxies: emergent empirical relations, feedback, and the evolution of very gas-rich systems

Federico I. Pelupessy¹, Padelis P. Papadopoulos²

ABSTRACT

We use time-varying models of the coupled evolution of the HI, H₂ gas phases and stars in galaxy-sized numerical simulations to: a) test for the emergence of the Kennicutt-Schmidt (K-S) and the H₂-pressure relation, b) explore a realistic H₂-regulated star formation recipe which brings forth a neglected and potentially significant SF-regulating factor, and c) go beyond typical galactic environments (for which these galactic empirical relations are deduced) to explore the early evolution of very gas-rich galaxies. In this work we model low mass galaxies ($M_{\text{baryon}} \leq 10^9 M_{\odot}$), while incorporating an independent treatment of CO formation and destruction, the most important tracer molecule of H₂ in galaxies, along with that for the H₂ gas itself. We find that both the K-S and the H₂-pressure empirical relations can robustly emerge in galaxies after a dynamic equilibrium sets in between the various ISM states, the stellar component and its feedback ($T \gtrsim 1$ Gyr). The only significant dependence of these relations seems to be for the CO-derived (and thus directly observable) ones, which show a strong dependence on the ISM metallicity. The H₂-regulated star formation recipe successfully reproduces the morphological and quantitative aspects of previous numerical models while doing away with the star formation efficiency parameter. Most of the HI \rightarrow H₂ mass exchange is found taking place under highly non-equilibrium conditions necessitating a time-dependent treatment even in typical ISM environments. Our dynamic models indicate that the CO molecule can be a poor, non-linear, H₂ gas tracer.

Finally, for early evolutionary stages ($T \lesssim 0.4$ Gyr) we find significant and systematic deviations of the true star formation from that expected from the K-S relation, which are especially pronounced and prolonged for metal-poor systems. The largest such deviations occur for the very gas-rich galaxies, where deviations of a factor $\sim 3-4$ in global star formation rate can take place with respect to those expected from the CO-derived K-S relation. This is particularly important since gas rich systems at high redshifts could appear as having unusually high star-formation rates with respect to their CO-bright H₂ gas reservoirs. This points to a possibly serious deficiency of K-S relations as elements of the sub-grid physics of star formation in simulations of structure formation in the Early Universe.

Subject headings: galaxies: numerical simulations – galaxies: spirals – galaxies: star formation – ISM: molecular gas – ISM: atomic gas – molecules: H₂,CO

¹Leiden Observatory, Leiden University, P.O. Box 9513, 2300 RA Leiden, The Netherlands

²Argelander-Institut für Astronomie, Auf dem Hügel 71, D-53121 Bonn, Germany

1. Introduction

In spite of the fact that the general character of the cycle through which galaxies convert their ISM to stars has been known for a long time, it has proven to be remarkably difficult to formulate a predictive theoretical framework for this process. Indeed, we know that throughout most of the Universe star formation takes place in molecular gas complexes (e.g. Solomon and Vanden Bout 2005; Omont 2007). The $\text{HI} \rightarrow \text{H}_2$ phase transition is conditioned by a combination of sufficiently high HI column densities and pressures, and consequently star formation tends to concentrate in high density regions, e.g. in the central parts of galaxies, in spiral arms or high-pressure concentrations of gas formed by bulk gas motions or swept up by the shocks from supernovae and stellar winds of OB associations. The link between molecular gas and star formation is so tight that it has even been used to infer the distribution of the former by that of the latter, when the CO- H_2 conversion factor was still considered very uncertain (Rana and Wilkinson 1986). In the Galaxy, where this link is best studied (e.g. Blitz 1997, and references therein), the latest results confirm star formation always taking place in CO-bright molecular clouds, even at very large galactocentric distances (Kobayashi et al. 2008). In other galaxies this tight association has been verified in all cases where sufficient angular resolution is available (e.g. Wong and Blitz 2002). Thus it is fair to say that *H_2 formation is a necessary prerequisite for star formation in galaxies*, and incorporating it in galaxy-sized numerical simulations of gas and stars is the single most important step currently missing from a realistic rendering of star formation in such models.

Following the early and widespread observational evidence establishing the H_2 -(star formation) link, the inclusion of the H_2 gas phase in numerical models of galaxies has occurred only recently (Pelupessy et al. 2006; Dobbs et al. 2006; Robertson and Kravtsov 2008), and the refinement of these models is an area of ongoing research. This is mainly due to the difficulty of tracking the dynamic and thermodynamic evolution of H_2 and its precursor phase, the Cold Neutral Medium HI ($n \sim 5-100 \text{ cm}^{-3}$, $T_k \sim 60-200\text{K}$, Wolfire et al. 2003) in galaxy-sized numerical models and due to the strong H_2 self-shielding complicating radiative transfer models of its far-UV radiation-induced destruction. The first problem has prevented most efforts from properly tracking the $\text{HI} \rightarrow \text{H}_2$ phase transition in galaxies without resorting to simplifying steady-state solutions (Hidaka and Sofue 2002; Robertson and Kravtsov 2008) (suitable only for quiescent galactic environments), or to semi-empirical multiphase models (e.g. Semelin and Combes 2002) with limited predictive value. The second problem confounds even numerical simulations tracking the $\text{HI} \rightarrow \text{H}_2$ phase transition in individual gas clouds where local approximations of the self-shielding HI/H_2 volume (necessary for numerically manageable solutions) can make the H_2 gas mass fraction a strong function of the chosen numerical resolution (e.g. Glover and Mac Low 2007). Finally a secondary, yet important problem of such single gas cloud simulations is posed by the constant boundary conditions assumed during their evolution, which are an unlikely setting for real gas clouds immersed in the ISM environment of a galaxy. In such environments cloud boundary conditions that powerfully influence the $\text{HI} \rightarrow \text{H}_2$ phase transition, such as the ambient FUV radiation field and pressure, change on timescales comparable or shorter than “internal” cloud dynamic and thermodynamic timescales, especially in vigorously star forming environments (e.g. Parravano et al. 2003; Wolfire et al. 2003; Pelupessy et al. 2006).

Despite the aforementioned difficulties the incorporation of the $\text{H}_2 \leftrightarrow \text{HI}$ gas phase interplay, and its

strong role as star formation regulator, in numerical models holds the promise of large improvements in their handling of galaxy evolution, and the possibility of unveiling new, hitherto neglected, aspects of star formation feedback on the ISM. In this paper we apply our numerical models for the coupled evolution of gas (HI, H₂) and stars (Pelupessy et al. 2006) to the evolution of low mass galaxies ($M_{\text{baryon}} < 10^9 M_{\odot}$) in order to explore two new key directions, the first of which is the emergence of two important empirical relations found for galaxies in the local Universe: the Kennicutt-Schmidt (K-S) and the H₂-pressure relation. Secondly we will make a investigation of very gas-rich systems (more typical of the Early Universe), and check whether the aforementioned relations remain valid during their evolution. The latter is of crucial importance given the prominent role such empirical relations are given in describing the sub-grid star-formation/gas interplay in cosmological simulations of galaxy evolution (where the resolution limitations imposed by the simulation of large volumes preclude a detailed description of star formation). Finally along with our original time-dependent treatment of the HI → H₂ phase transition we also include the CO molecule, allowing direct comparisons to the *observed* H₂ gas distributions, and a new independent investigation of the CO-H₂ relation within the dynamical setting of an evolving galaxy.

The structure of our work is as follows: in section 2 we present relevant features of the model, show semi-analytical predictions for the H₂-pressure relation, and formulate the extension of the model so that includes CO, in section 3 we present our detailed numerical simulations, and investigate the K-S, H₂-pressure and CO-H₂ empirical relations. In section 4 we investigate and discuss the validity of the important K-S relation during early galaxy evolution stages, and for very gas-rich systems. We then summarize our conclusions in section 5.

2. Incorporating the molecular gas phase: a dynamical approach

The HI → H₂ phase transition in galaxies, as catalyzed by dust grains, have been studied extensively ever since the strong self-shielding nature of H₂ in its dissociation by far-UV (FUV) photons has been recognized (Spitzer and Jenkins 1975; Savage et al. 1977; Federman et al. 1979). These theoretical (Elmegreen 1989, 1993; Papadopoulos et al. 2002), and observational (Honma et al. 1995) studies made clear that ISM pressure, ambient FUV field, as well as metallicity play major roles in the HI → H₂ phase transition. The role of pressure in particular has been highlighted over a wide range of galaxy properties (Blitz and Rosolowsky 2004), and quantified in an empirical H₂-pressure relation derived by Blitz and Rosolowsky (2006). Such a relation (hereafter B-R relation) along with the well-established K-S relation (Kennicutt 1989, 1998) are the most encompassing observational benchmarks that galaxy models must pass before they can be trusted in their predictions. Moreover, by linking gas and star formation (K-S relation), and the H₂ phase (the true star formation fuel) to “macroscopic” ISM environmental parameters such as pressure (B-R relation) these empirical relations are natural choices for any sub-grid formulation that relates gas and star formation in simulations of cosmological volumes where sub-grid recipes for star physics at kpc scales become necessary.

Currently there is no evidence that the K-S and B-R relations hold in the extreme and very gas-rich star

forming galaxies discovered at high redshifts (e.g. Walter et al. 2003), and there is even tentative evidence that the K-S relation obtained in the local Universe may not be applicable in UV/optically selected galaxies at high redshifts (Tacconi et al. 2008). Detailed galaxy-sized simulations of gas and stars are thus important tools for exploring the robustness and possible limitations of these empirical relations in a systematic fashion. Key features of our galaxy-sized TREE/SPH numerical models of gas+stars that make them appropriate for such purposes are:

- Non-equilibrium treatment of the gas thermodynamics, resulting in gas with $(n, T_{\text{kin}}) \sim (0.1 \text{ cm}^{-3}, 10^4 \text{ K})$ (the WNM HI phase) to $(n, T_{\text{kin}}) \sim (100 \text{ cm}^{-3}, 40 \text{ K})$, (i.e. the CNM HI and the resulting H_2 phase).
- Tracking temporally and spatially varying radiation fields (profoundly influencing the $\text{HI} \rightarrow \text{H}_2$ phase transition within a galaxy) using time-dependent stellar evolution libraries.
- A time-dependant sub-grid physical model of the HI/H_2 mass exchange that readily incorporates the varying ambient conditions expected for the ISM within an evolving galaxy.
- Star formation controlled by a Jeans-mass instability criterion.

The latter is enabled by the fact that our code tracks the gravitational and thermodynamical state of the gas and can identify gravitationally unstable regions down to the temperatures and densities typical of Giant Molecular Clouds (GMCs). It is in such regions that strong observational evidence and theoretical considerations (e.g. Elmegreen 2000, 2002) suggests that star formation occurs. Finally, note that given the continuous mass exchange between the WNM and the CNM gas phase, and the non-equilibrium conditions often found for the former even for quiescent environments in the Milky Way (Wolfire et al. 2003), any successful time-dependent treatment of the $\text{HI} \leftrightarrow \text{H}_2$ mass exchange within evolving galaxies must track the ISM thermodynamics.

2.1. The H_2 model

The subgrid cloud structure model used by Pelupessy et al. (2006) to describe the $\text{HI} \leftrightarrow \text{H}_2$ mass exchange is constructed using widely observed ISM scaling laws (Larson 1981; Heyer and Brunt 2004), shown to hold generally for gas clouds virialized under a background pressure (Elmegreen 1989). A major development since our first use of this sub-grid cloud representation in our numerical models is that these scaling laws have now been found to hold for extragalactic GMCs as well (Bolatto et al. 2008). Below we describe its main features, while more details can be found in Pelupessy et al. (2006).

For a cloud with radius R , mean density $\langle n \rangle$, and internal density profile $n(r) \propto 1/r$, consisting of a molecular core and an outer HI gas layer of a $\text{HI} \rightarrow \text{H}_2$ transition column density $N_{\text{tr}}(\text{HI})$, under irradiation by an external stellar UV field the molecular fraction can be expressed as

$$f_{\text{H}_2} \equiv \frac{M(\text{H}_2)}{M_c} = \exp \left[-3 \frac{N_{\text{tr}}}{\langle n \rangle R} \right]. \quad (1)$$

Here we will assume that the gaseous ISM is composed of structure conforming to the widely observed density-size scaling relation (Larson 1981; Pelupessy et al. 2006),

$$\langle n \rangle R = 4.7 \times 10^{21} \left(\frac{P_e/k_B}{10^4 \text{ K cm}^{-3}} \right)^{1/2} \text{ cm}^{-2}. \quad (2)$$

Hence, a calculation of the thickness of the neutral layer $N(\text{HI})$ gives the local molecular fraction from equations 1 and 2. For this transition column density $N(\text{HI})$ a differential equation can be formulated that describes the time evolution

$$\tau_f \frac{d\sigma N_{\text{tr}}}{dt} = r_{\text{dis}} e^{-\sigma N_{\text{tr}}} - \sigma N_c \left(e^{\sigma N_{\text{tr}}/\sigma N_c} - 1 \right), \quad (3)$$

where $\tau_f = 1/(2nR_f)$ is the H_2 formation timescale. The H_2 formation rate function R_f depends on temperature T_k , metallicity Z , and a normalization parameter μ (encoding the uncertainties inherent in its absolute value, with $\mu = \mu_0 = 3.5$ corresponding to the Jura (1974) formation rate of $R_f \sim 3 \times 10^{-17} \text{ s}^{-1}$ at $T = 100\text{K}$), as

$$R_f = 3.5 \times 10^{-17} \mu Z \left(\frac{T_k}{100 \text{ K}} \right)^{1/2} S_H(T_k) \gamma_{\text{H}_2} \text{ cm}^3 \text{ s}^{-1}. \quad (4)$$

The function $S_H(T_k)$ expresses the HI sticking probability on a dust grain and forming an H_2 molecule that then detaches itself from the grain with a probability γ_{H_2} . Here we adopt $S_H(T_k) = [1 + (k_B T_k / E_o)]^{-2}$ ($E_o/k_B \sim 100 \text{ K}$) obtained by the study of Buch and Zhang (1991) and $\gamma_{\text{H}_2} \sim 1$. The dimensionless parameter

$$r_{\text{dis}} \equiv \frac{G k_o}{n_e R_f} \Phi \quad (5)$$

measures the relative balance of the H_2 dissociation versus the H_2 formation, with $k_o = 4 \times 10^{-11} \text{ s}^{-1}$ being the (unshielded) H_2 dissociation rate and G the far-UV radiation field in Draine field units ($2 \times 10^7 \text{ photons s}^{-1} \text{ cm}^2$ between 11.2 and 13.6 eV, Draine 1978). The dimensionless factor Φ is an integral of the self-shielding function over the H_2 column, which encompasses the details of H_2 self-shielding (Goldshmidt and Sternberg 1995; Pelupessy et al. 2006). For a detailed explanation of the solution of Equation 3 within our dynamical model and key dependencies of the $\text{HI} \rightarrow \text{H}_2$ phase transition the reader is referred to Pelupessy et al. (2006). The numerical simulations presented in the section 3 use the solution to the fully time-dependent Equation 3. For the moment we will consider the equilibrium solutions first to gain some qualitative insight in the B-R relation.

2.2. Equilibrium results: The B-R relation

The equilibrium transition column density for the fiducial case where the density, radiation field etc of a given patch of ISM is constant in time, is given by (Pelupessy et al. 2006),

$$N_{\text{tr}}(\text{HI}) = \frac{\nu}{\sigma_{\text{FUV}}} \ln \left(1 + \frac{3}{2\nu} \frac{G k_o}{R_f n} \Phi \right), \quad (6)$$

where $\nu = nR\sigma_{FUV} / (\frac{3}{2} + nR\sigma_{FUV})$. Together with Equations 1 and 2 one can calculate the corresponding equilibrium molecular to neutral ratio $R_m \equiv f_{\text{H}_2} / f_{\text{HI}} = f_{\text{H}_2} / (1 - f_{\text{H}_2})$. The latter depends only on the following local conditions of an ISM gas parcel: the density (n), temperature (T_k), metallicity (Z) and impinging UV radiation field (G) as well as the local turbulent velocity field with velocity dispersion σ through the total external pressure

$$P_e/k_B = n(T + 54\sigma^2) \text{ Kcm}^{-3} \quad (7)$$

(needed in Equation 2). In Figure 1 we show the resulting R_m - P_e relation and compare it to the observed one (Blitz & Rosolowsky 2006). The shaded regions indicate the scatter in the observational B-R relation, both for the individual measurements in a given galaxy as well as between different galaxies. For interpreting the plots in Figure 1 we need to consider the following: a) the observed B-R relation is one between the projected molecular-atomic ratio and midplane pressure (estimated from projected quantities), and thus not exactly the same as the theoretical points in Figure 1 that use the volume-averaged local R_m ratio and pressure, and b) these results correspond to ISM equilibrium. In practice the ISM may not be even in an approximate equilibrium, especially for low density/low pressure regions where the timescales to equilibrium are the longest. For the moment we defer discussion of projection and non-equilibrium effects to the investigation of realistic galaxy models in Section 3.

A number of important points becomes apparent from the panels in Figure 1 namely:

- for a wide range of parameters a B-R type of relation does emerge. Variations in temperature (fig. 1a), velocity dispersion (fig. 1b), and radiation field (fig. 1d) as well as the formation rate parameter μ (fig. 1c) have only a minor effect. This shows that a (B-R)-type relation is plausible from a theoretical point of view, while its various functional dependences remain within its observational scatter expected within and between galaxies.
- Metallicity has a more pronounced effect on the H_2 -pressure relation. Figure 1e shows that for low metallicity environments the theoretical relation tends to fall significantly below and outside the nominal range, while it steepens at low pressures. Systematic studies of the B-R relation in low metallicity galaxies may reveal such deviations. Note however that it is still possible to shift the theoretical points back to the nominal B-R relation by assuming e.g. a lower radiation field.
- The plotted relations in general have slopes and normalization similar to the observed B-R relation, but not necessarily equal (though remaining mostly within the expected observational scatter). Introducing a secondary dependence of one of the other variables on pressure can easily produce exact matches of the B-R slope. In a stationary model there is no unique way of doing this, though. For example, postulating a G dependency on pressure ($G \propto P^{1/2}$) or a velocity dispersion dependency $\sigma \propto P^{1/4}$ or some suitable combination of those will result in a relation with a slope close to the observed value (~ 0.92). While such secondary relations are plausible (e.g. ISM environments with large pressures tend to host more vigorous star-formation and will thus have higher G 's), it is uncertain whether they indeed emerge in a more realistic time-dependent galaxy-size model of gas and stars.
- The pressure dependence of R_m expressed in the observational B-R relation could effectively boil

down solely to a density dependence given that midplane pressures observationally are estimated using a constant velocity dispersion (the dominant pressure contributor in the CNM ISM). Previous work though has deduced a direct dependence of R_m on the ISM pressure (Elmegreen 1993). To distinguish between these possibilities in Figure 1f we investigate the H_2 -pressure relation at constant density (i.e. varying the pressure only through the velocity dispersion). It can be seen that the B-R relation is still present but tends to flatten (especially for high densities) to $\propto P^{0.5}$. Additional sources of pressure (magnetic fields, ram pressure, shocks) may be expected to behave similarly: increasing R_m but not as strongly as an increase in density would do it.

Finally, unlike the investigation of B-R relation a similar one for the K-S relation must involve the full dynamical treatment allowed by our models given that in our approach star formation is controlled by the Jeans mass criterion (a dynamical one) rather than any parametric formulation.

2.3. The CO model

Direct detection of H_2 gas is difficult given that its lowest transition $S(0) : J_u - J_l = 2 - 0$ at $28\mu\text{m}$ still has $E_{20}/k_B \sim 510\text{K}$, much too high to be substantially excited by the typically much colder H_2 gas ($T_k \sim 15 - 60\text{K}$). This fact, along with its small Einstein coefficient ($A_{20} = 2.94 \times 10^{-11} \text{ s}^{-1}$), diminishes its luminosity, while at $28\mu\text{m}$ the Earth's atmosphere is mostly opaque, further compounding the observational difficulties of its detection. These difficulties made the next most abundant molecule after H_2 itself, CO (with $[\text{CO}/\text{H}_2] \sim 10^{-4}$ for Solar metallicities) and its easily excited rotational lines (mostly CO $J=1-0$ at 115GHz with $E_{10}/k_B \sim 5.5\text{K}$ and $n_{\text{crit}} \sim 400\text{cm}^{-3}$) the molecular gas tracer of choice via the so-called CO- H_2 conversion factor (Dickman et al. 1986; Solomon et al. 1987, e.g.) It must be noted that *all* fundamental relations that involve the H_2 gas distribution in galaxies have been deduced for CO-bright H_2 gas. This may not encompass the bulk of the molecular gas phase, especially in metal-poor and/or FUV-aggressive ISM environments (Maloney and Black 1988; Pak et al. 1998; Bolatto et al. 1999). Such conditions can be found in spiral disks at large galactocentric distances because of well-known metallicity gradients (e.g. Henry 1998; Garnett 1998, and references therein), as well as in dwarf irregular galaxies (Israel 1997; Madden et al. 1997). Finally metal-poor systems with significant star formation rates (and thus strong FUV radiation fields) such as Ly-break galaxies are also known at high redshifts (Steidel et al. 1999).

Thus in our models it would be instructive to examine the specific distribution of the CO-rich, conventionally observable H_2 gas. Moreover, by tracking the evolving ISM environment in which real gas clouds are immersed, we can identify conditions regions and epochs in which CO-bright H_2 gas in galaxies may significantly underestimate its true distribution during the evolutionary track of a galaxy. Including it in simulations allows a dynamic examination of the CO- H_2 relation, contrasting and complementing those based on static Photo-Dissociation Regions (PDRs) models (Pak et al. 1998; Bolatto et al. 1999).

For the CO model we adopt a similar model as for H_2 : the size of the CO dominated region within a spherical cloud can be estimated by considering the width of the C^+ layer that surrounds a mixed C^0 , CO inner region (Papadopoulos et al. 2004, and references therein). The dominant reaction channels for the

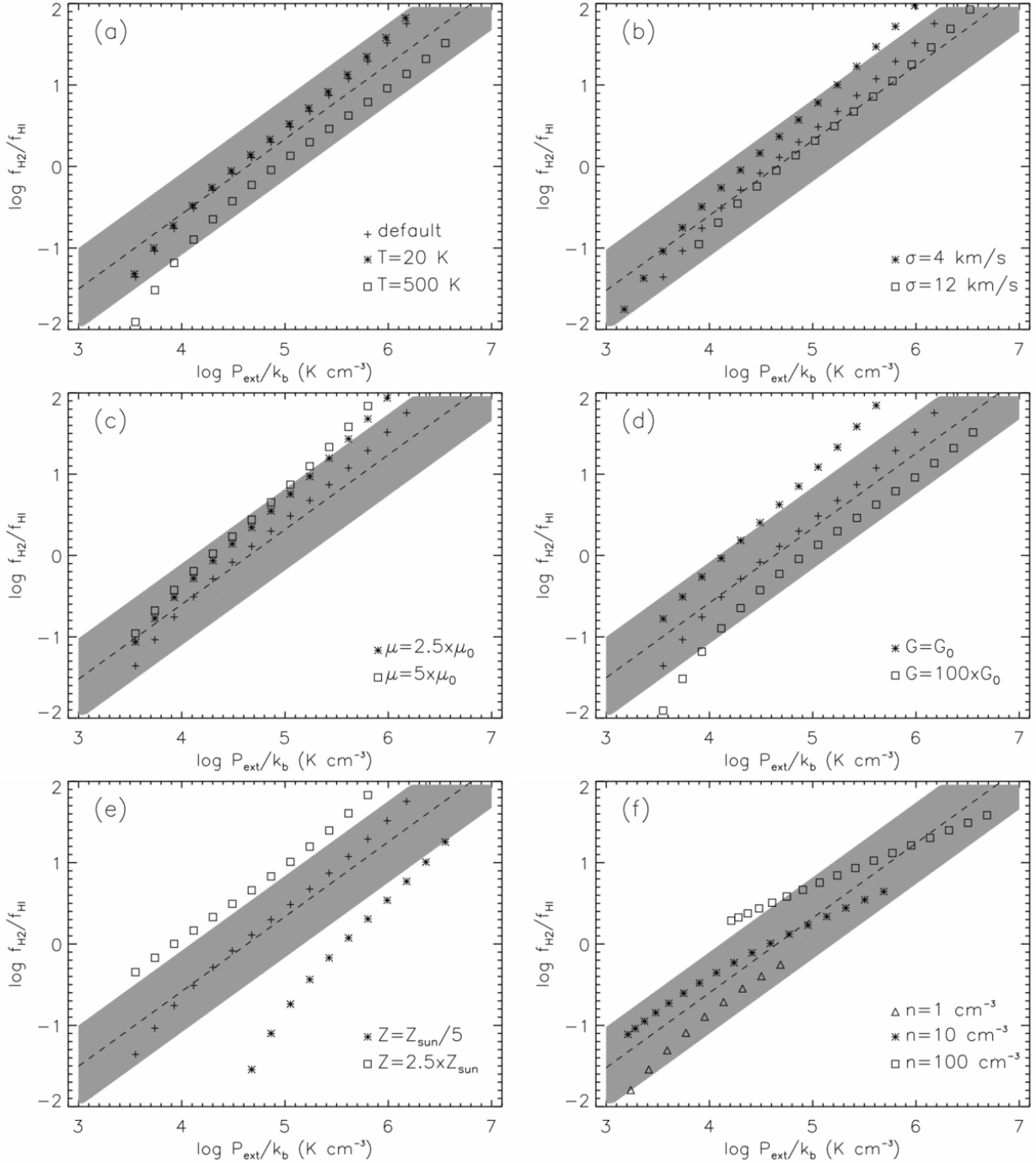


Fig. 1.— Equilibrium expectations for $f_{\text{H}_2}/f_{\text{HI}}$ (points) for a range of physical parameters (section 2) versus the observed B-R relation and its scatter (dashed line and shaded area). In panels (a)-(e) the plus symbols are plotted with the same default set of parameters: $T = 100\text{K}$, $\sigma = 8$ km/s, $\mu = \mu_0$, $G = 10 \times G_0$ and $Z = Z_\odot$.

formation and destruction of C^+ that determine its layer are:



Following Röllig et al. (2006), the radius r_+ beyond which the gas is C^+ -dominated in spherical FUV-illuminated clouds with a uniform density n can be estimated from

$$3 \times 10^{-10} s^{-1} G E_2[\xi_{FUV} A_v(r_+)] = n_H (a_c X_c + 0.5 k_c), \tag{9}$$

where $X_c = [C/H] = 1.4 \times 10^{-4} Z$, the factor $\xi_{FUV} \sim 2-4$ accounts for the absorption at FUV wavelengths, and E_2 is the second order exponential integral

$$E_2[\xi_{FUV} A_v(r_+)] = \int_1^\infty \frac{e^{-\mu \xi_{FUV} A_v(r_+)}}{\mu^2} d\mu. \tag{10}$$

The recombination and radiative association rate coefficients for the reactions: $C^+ + e^- \rightarrow C + \nu$ and $C^+ + H_2 \rightarrow CH_2^+ + \nu$ that destroy C^+ are $a_c = 3 \times 10^{-11} \text{ cm}^3 \text{ s}^{-1}$ and $k_c = 8 \times 10^{-16} \text{ cm}^3 \text{ s}^{-1}$, while the extinction A_v from r_+ to the edge of the cloud R , given by (again for a $n \propto r^{-1}$ density profile)

$$A_v(r_+) = 0.724 \sigma_v Z n R \ln \left(\frac{R}{r_+} \right). \tag{11}$$

The product nR can be eliminated using the linewidth-size relation Equation 2. Equation 9 is solved numerically for r_+ by simple root finding. From this we obtain the CO-bright part of the H_2 cloud through $f_{CO} = (r_+/R)^2$. Given the fact that CO formation happens at much higher densities ($n \gtrsim 1000$), and correspondingly shorter timescales, than H_2 formation, the stationary treatment adopted for the CO chemistry is appropriate.

3. The dynamical model: gas+stars galaxy simulations

3.1. Simulation code

The code calculates gravity using a TREE code (Barnes and Hut 1986) and gas dynamics using the SPH formalism (see e.g. Monaghan 1992), and the conservative formulation of Springel and Hernquist (2002). An advanced model for the ISM medium is used, a star formation recipe based on a Jeans mass criterion, and a well-defined feedback prescription. The code is described and tested in detail in Pelupessy (2005); Pelupessy et al. (2004), below we will only give a brief description of the relevant physical ingredients.

3.1.1. ISM model

Our ISM model is similar, albeit simplified, to that of Wolfire et al. (1995, 2003). We solve for the thermal evolution of the gas including a range of collisional cooling processes, cosmic ray heating and

ionization. From the viewpoint of our application here the most important feature is the tracking of the WNM and CNM HI phases. The latter is where high densities and low temperatures allow the H₂ molecules to form and survive, with the H₂ gas phase (Section 2) then naturally completing the ISM treatment.

The FUV luminosities of the stellar particles, which are needed to calculate the photoelectric heating from the local FUV field, are derived from Bruzual & Charlot (Bruzual A. and Charlot 1993, and updated) population synthesis models for a Salpeter IMF with cutoffs at 0.1 M_⊙ and 100 M_⊙. In the present work we do not account for dust extinction of UV light, other than that from the natal cloud: for a young stellar cluster we decrease the amount of UV extinction from 75% to 0% in 4 Myr (see Parravano et al. 2003).

3.1.2. Implementation of the H₂ model

The gas particles in the code are assigned, in addition to the usual density ρ , internal energy u , etc, a varying local molecular gas fraction f_m . We then use Eq. 3 to track the evolution of σN_{tr} , and thus f_m (through eq. 1 and eq. 2), during a simulation timestep dt . If the temperatures are too high for H₂ formation to occur we solve for the evolution of f_m using pure photo-destruction while for $T_k > 3000$ K, we treat the collisional destruction process of the remnant molecular gas using rates from Martin et al. (1998).

The density that enters in those equations is assumed to be the mean density $\langle n \rangle$ given by the SPH density at the particle position, and the temperature the particle temperature (both taken constant during the timestep). The radiation field is calculated from the distribution of stars, assuming no other extinction apart from that in the natal clouds. For the macroscopic pressure P_e we need the local velocity dispersion σ . For this we take the formal SPH estimate

$$\sigma_j^2 = \sum_i \frac{m_i}{\rho_j} (v_i - \langle v \rangle_j)^2 W(|r_{ij}|, h_j) \quad (12)$$

with v_i and m_i the particle velocities and masses, $\langle v \rangle_j$ the local bulk velocity.

3.2. Star formation: SN feedback, and H₂ as an additional SF regulator

The coldest and densest gas in our simulations is found in the CNM phase with the H₂ formation occurring on the formation timescales of the Giant molecular clouds (GMC) complexes embedded in this phase. Following gravitational instabilities further “down” in the CNM phase would require additional physics (e.g. CO and H₂O cooling of dense molecular cores, the emergence of the IMF, etc) as well as demanding much higher numerical resolution, currently unattainable. At this point it is appropriate to introduce a prescription to further track the star formation process.

The first assumption we make is that star formation is governed by the gravitational instability of gas clouds, with a region considered unstable to star formation if its local Jeans mass $M_J < M_{\text{ref}}$, where $M_{\text{ref}} \approx 10^{4-5} M_{\odot}$ is a reference cloud mass. The exact value of M_{ref} is not important (Gerritsen 1997), and provided that it is always well-resolved by our simulation this star-formation criterion precludes the

emergence of numerical artifacts that can result from insufficient resolution of the Jeans mass. Moreover an M_{ref} smaller than typical GMC masses (as the chosen values are) makes the Jeans instability criterion select conditions “deep” into the dense parts of the CNM phase. This makes this criterion a good assumption for the onset of star formation, mirroring the irreversibility of the (gas) \rightarrow (stars) transition observed in nature once dense CNM clouds form. Once a region is deemed unstable it proceeds towards star formation by converting some fraction ϵ_{SF} of the gas particle to stars after a delay time. This delay is taken to be proportional to the local free fall time: $\tau_{\text{sf}} = f_{\text{sf}} t_{\text{ff}} = \frac{f_{\text{sf}}}{\sqrt{4\pi G\rho}}$. The delay factor f_{sf} is uncertain, but from observations a value $f_{\text{sf}} \approx 10$ seems necessary to account for the observed inefficiency of star formation (Zuckerman and Evans 1974). The actual rate of star formation is then determined by balance between gas cooling and the far-UV and SN heating. We will refer to this star formation model as the Simple Delay (SD) model.

Our ISM model allows to set the local H_2 gas mass fraction as star formation regulator in the dynamical setting of an evolving galaxy. Irrespective whether H_2 formation ahead of star formation is incidental (e.g. cold and dense gas forms H_2 on its “way” to gravitational collapse and eventual star formation) or instrumental (e.g. H_2 *must* form first so that CO and other powerful molecular coolants can form and “drive” the gravitational collapse further towards denser and colder ISM regimes), this is a very important step towards a better, much more realistic rendering of the star formation process in numerical models. We implement this molecular regulated (MR) star formation by converting the molecular (f_{m}) mass fraction of an unstable (i.e. $M_{\text{J}} < M_{\text{ref}}$) gas particle to stars (with a minimum value of $f_{\text{m}} = 0.125$, corresponding to a particle mass of $\sim 60M_{\odot}$, to avoid the creation of very small star particles). Unlike the (SD) recipe that needs an adhoc ϵ_{SF} value, the (MR) one contains a physical basis for this part of the star formation modeling and thus no longer needs a star formation efficiency parameter ϵ_{SF} .

The mechanical energy output of stars is reasonably well known but it has been proven difficult to include its feedback (i.e. supernovae and stellar winds) self-consistently in galaxy-sized ISM simulations. The reason for this is that the effective energy of such feedback depends sensitively on the energy radiated away in thin shells around the bubbles created, which would need prohibitively high resolution to follow. In SPH codes there have been conventionally two ways to account for feedback: by changing the thermal energy input and by acting on particle velocities. Both are unsatisfactory, as the thermal method suffers from overcooling (Katz 1992) and the kinetic method is too efficient in disturbing the ISM (Navarro and White 1993). Here we use a method based on the creation of *pressure particles* that act as normal SPH particles in the limit of the particle mass m_p going to zero (Pelupessy et al. 2004; Pelupessy 2005). Such a pressure particles is associated with every newly formed star particle and will receive its feedback energy, acting on the surrounding gas particles through the usual SPH particle forces in the limit that $m_p \rightarrow 0$ while simultaneously keeping the product of particle mass and specific thermal energy, $m_p \times u_p$, fixed. The thermal evolution (the time dependence of $m_p \times u_p$) is specified by adiabatic expansion and the energy input from young stars. For this energy injection rate we take $\dot{E} = \epsilon_{sn} n_{sn} E_{sn} / \Delta t$, with $E_{sn} = 10^{51}$ erg, $\epsilon_{sn} = .1$, $n_{sn} = 0.009$ per M_{\odot} and $\Delta t = 3 \times 10^7$ yr. The efficiency ϵ_{sn} thus assumes that 90% of the energy is radiated away in thin, dense shells.

3.3. Galaxy models

The galaxy models we use stem from the analytic disc galaxy models of Mo et al. (1998), constructed as described in Springel et al. (2005). They consist of a disk consisting of a stellar and a gaseous component embedded in a dark halo. The stellar disk has an exponential disk radial profile (with scale length R_*),

$$\rho_{disk}(R, z) = \frac{\Sigma_0}{2h_z} \exp(-R/R_*) \operatorname{sech}^2(z/h_z). \quad (13)$$

The gas disk is set up in vertical hydrostatic equilibrium with a surface density profile consisting of an exponential component (so proportional to the stellar density) and a more extended component

$$\Sigma = \Sigma_g / (1 + R/R_g) \quad (14)$$

cutoff at a radius $8 \times R_g$. Note that this distribution is necessary to match closer the observed gas distributions that typically extent well beyond the stellar ones. Apart from the radial profiles the stellar and gas disk are initialized as smooth initial conditions and the gas is setup with a constant temperature (8000K). Finally the dark halo has an Hernquist profile

$$\rho_{halo}(r) = \frac{M_{halo}}{2\pi} \frac{a}{r(r+a)^3}. \quad (15)$$

The Hernquist scale parameter is related to the more familiar scale parameter r_s and the concentration index c of Navarro, Frenk and White (NFW) profiles (see Springel et al. 2005, for details). We do not include a bulge component here.

We take models of different size by choosing the total baryonic mass, the disk being a mass fraction f_{baryon} of the total mass, and consider galaxies ranging in mass from $M_{baryon} = 10^8 M_\odot$ to $M_{baryon} = 10^9 M_\odot$, with $f_{baryon} = 0.041$. The smaller scale is representative of dwarf galaxies and the bigger of small disk galaxies. We vary the gas mass fraction of the disk from $f_{gas} = 0.5$ (for the low mass model) to $f_{gas} = 0.2$ (for the high mass model), roughly mirroring the observed correlation between gas fraction and galaxy size. The total halo virial mass is fixed by $M_{vir} = M_{baryon} / f_d$ ($M_{vir} = M_{halo} + M_{baryon}$), which gives the virial velocity and radius through the relations

$$M_{vir} = \frac{v_{vir}^3}{10GH(z)}, \quad (16)$$

$$R_{vir} = \frac{v_{vir}}{10GH(z)}, \quad (17)$$

$$(18)$$

assuming a virial overdensity $\Delta = 200$. Determining the c index gives the halo scale length. The metallicity of each model will be taken to be constant during the run, but we will consider different metallicities, namely models at solar metallicity Z_\odot and at $0.2 \times Z_\odot$. These models are summarized in Table 1 as models A1 to C1. Other parameters of the models are not varied here: we fix the spin parameter at $\lambda = 0.05$. The λ implicitly determines the scale lengths of the gas and stellar disk, as the angular momentum in the disk is assumed to scale with the angular momentum in the parent halo. The scale height of the stellar component is taken to be a fraction of the radial scale length: $z_h = 0.2 - 0.4 \times R_*$. The galaxy models are realized with

mass resolutions for the gas particles of $200-10^3 M_{\odot}$, also given in Table 1. Finally two models with very high gas mass fractions are also run (D1 and E1), representing extreme systems expected at early epochs of galaxy evolution. For these we set an initial gas mass fraction of $f_{\text{gas}} = 0.99$.

3.4. Runs

In addition to different galaxy models A1-E1 we also test our two different star formation recipes (MR and SD) described in Section 3.2. Each model is run well beyond the time strong evolutionary effects take place (investigated in section 4) and until a dynamic equilibrium for the star formation sets in. At this evolutionary point, i.e. ~ 1 Gyr of simulation time after the start of the simulation, we analyze the resulting gas distributions. Given that at present chemical enrichment effects (influencing ISM thermodynamics and H_2 formation) and cosmological infall are not included, evolving our models for much longer timescales is of limited value, simply resulting in a steady depletion of their gas reservoirs.

3.5. Results

Table 2 gives an overview of the molecular gas fractions and star formation rates of our runs. From this table it can be seen that the low metallicity models ($Z = Z_{\odot}/5$, A B and E models) have a molecular fraction $f_m \sim 0.03-0.05$, while the models at solar metallicity (C and D models) reach up to $f_m \sim 0.4-0.6$. Models with the same metallicity reach similar molecular fractions while the structural parameters of the galaxy models seem to have only a minor influence on the global molecular fraction, at least over the limited range explored here. It is also important to point out that the SPH particle mass has little effect on the basic physical quantities examined here, suggesting that adequate numerical resolution has been reached to describe the physical mechanisms considered.

A comparison of SD and MR star formation recipes shows that the latter results in less molecular gas and increased SFRs. A useful measure of the star formation efficiency is the gas consumption timescale $\tau_x = M_x/SFR$, also given in Table 2, and calculated separately for atomic and molecular hydrogen. For the low metallicity models we find typically $\tau_{\text{HI}} \sim 5-8$ Gyr and $\tau_{\text{H}_2} \sim 0.15-0.3$ Gyr, while for the high metallicity models the timescales for HI and H_2 become comparable, with $\tau_{\text{HI}} \sim 1.5-3$ Gyr and $\tau_{\text{H}_2} \sim 0.6-5$ Gyr. These results seem largely independent of the SF model adopted and reflect a general characteristic of low-Z versus high-Z systems, namely that the former are much more WNM-dominated than the latter. This can be seen in the last column of Table 2, where the $M_{\text{CNM}}/M_{\text{WNM}}$ ratio is also tabulated (CNM is taken to be all gas colder than 1000 K, WNM gas with $1000 < T < 10000$). For systems that are WNM-dominated, hydrogen will be overwhelmingly atomic, and the large disparity between the HI and H_2 gas consumption timescales simply reflects the one between atomic and molecular gas reservoirs and the fact no Jeans-unstable regions occur in the WNM phase and thus star formation can never directly “consume” its mass. For high metallicities the mass allocation between WNM HI and CNM HI and H_2 becomes more even and so are the corresponding consumption timescales. Note that for the SD model alone one might be tempted to conclude that the short

H_2 gas consumption timescale at low Z (or equivalently the low f_m) has something to do with the fact this model is formulated independent of molecular gas (thus unrealistically converting gas into stars before molecules can form). This is not the case: the MR model has *lower* consumption timescales at low Z (partly due to a general higher SF), and lower molecular fractions. It seems that even in the MR model the outcome of the star formation model is not constrained by the chemistry of H_2 formation but by the conversion of WNM to CNM. The difference between high metallicity gas and low metallicity gas is that molecular gas forms in smaller reservoir of CNM gas. Once there, evolution to star formation occurs faster than the large scale processes driving gas down to the CNM, so it is not necessary for a large reservoir of H_2 to form.

Compared with the SD model the MR star formation model has a $\sim 50\%$ lower molecular fraction and a $\sim 50\%$ higher rate of SF. This increase in efficiency of SF in terms of its molecular mass means that the H_2 gas consumption timescale is a factor $\sim 3-4$ times shorter. The reason for the smaller amount of H_2 gas is that the MR recipe selects SF sites that are on average denser CNM regions (where H_2 forms), and that these regions are then converted to stars, resulting in a more efficient consumption of molecular gas. At least globally, $M(\text{HI}+\text{H}_2)/\text{SFR}$ seems relatively insensitive to the SF recipe chosen. Given that stars form unequivocally only out of the H_2 -rich regions of the CNM phase this suggests that any self-regulating mechanism responsible for distributing the gas between the SF and the non-SF phase remains broadly similar in these two SF recipes. Of course we must reiterate that the MR star formation recipe is the more physical of the two, doing away with the adhoc ϵ_{SF} parameter typically used in numerical models. The emergence of a robust global efficiency $M(\text{HI}+\text{H}_2)/\text{SFR}$ out of dynamic galaxy models where only cold, dense, and H_2 -rich gas is allowed to form stars confirms the trustworthiness of (K-S)-type phenomenological relations. This is because the latter often relate the total gas mass to star formation, irrespective of its thermodynamic state or molecular gas fraction.

In Figures 2 and 3 we show the gas distribution from the simulation snapshots of models A1-E1. The top row of Figure 2 shows the HI gas maps obtained from projecting the neutral mass fraction of the particles for runs using the SD star formation model. In the middle row the molecular gas distribution obtained from f_m directly is shown, while the bottom row shows the maps for the CO-rich H_2 distribution (determined as in Section 2.3). Figure 3 shows the equivalent maps for the MR star formation runs. Some features of these maps are common across different models. For example the panels for the C1 run (spiral galaxy/solar metallicity, middle panels) show the frothy appearance of the neutral gas distribution typical for a star forming ISM. Comparing the HI and H_2 maps we see from the enhanced contrast of the molecular map that the H_2 tends to concentrate in the higher density regions. In the outer galaxy regions the H_2 distribution cuts off before the HI distribution and the smoothness of the gas distribution shows little feedback from stars. The third row panels shows the CO distribution concentrated towards high column densities in the central regions and dense clumps. Much the same pattern is visible for the equivalent low metallicity run B1. Low metallicity means less H_2 and CO formed, with CO restricted to the very highest density clumps. Note also that there is a big smooth region where star formation and H_2 are absent, a pattern repeated in the A1 run (note that the linear scale of the maps are different). The pure gas models (two right most panels in figs. 2, 3) are stable despite the high gas content, stabilized by supernova feedback (Springel et al. 2005).

The resulting gas distribution for the MR star formation model (fig. 3) is generally similar to the SD

Table 1: Overview of galaxy model parameters. The letters A-E indicate different structural properties and/or metallicities while numbering indicates different resolutions used on otherwise identical models. The gas distributions of models D1 and E1 consist of equal mass exponential and extended disk, the other models consist purely of the extended distribution eq. 14

Model	M_{baryon}	M_{vir}	f_{gas}	m_{par}	Z
A1	10^8	2.3×10^9	0.5	200	0.2
A2	10^8	2.3×10^9	0.5	500	0.2
B1	10^9	2.3×10^{10}	0.2	500	0.2
B2	10^9	2.3×10^{10}	0.2	1000	0.2
C1	10^9	2.3×10^{10}	0.2	500	1.
D1	10^9	2.3×10^{11}	.99	1000	1.
E1	10^9	2.3×10^{11}	.99	1000	0.2

Table 2: Results: molecular masses and fractions for runs.

Run	SF model	M_{gas} ($10^7 M_{\odot}$)	M_{HI} ($10^7 M_{\odot}$)	M_{H_2} ($10^7 M_{\odot}$)	f_{H_2}	R	SFR (M_{\odot}/yr)	τ_{HI} (10^9 yr)	τ_{H_2} (10^9 yr)	$\frac{f_{\text{CNM}}}{f_{\text{WNM}}}$
A1	SD	4.5	4.0	0.2	0.045	0.05	0.005	5.8	0.3	0.64
	MR	4.4	4.1	0.1	0.023	0.024	0.006	4.7	0.11	0.41
A2	SD	4.4	4.0	0.21	0.047	0.052	0.005	6.0	0.31	0.64
	MR	4.2	3.8	0.1	0.024	0.027	0.006	4.7	0.13	0.4
B1	SD	19.0	17.	0.86	0.045	0.049	0.01	11.8	0.58	0.61
	MR	19.0	17.	0.4	0.02	0.022	0.015	7.8	0.17	0.39
B2	SD	19.1	17.	0.84	0.044	0.048	0.009	12.3	0.59	0.59
	MR	18.6	17.	0.34	0.02	0.02	0.015	8.4	0.16	0.38
C1	SD	18.6	6.7	11.	0.61	1.7	0.014	3.2	5.4	5.28
	MR	17.1	11.	5.4	0.3	0.49	0.031	2.5	1.2	1.81
D1	SD	88.	41.	46.	0.52	1.1	0.14	2.0	2.2	3.06
	MR	76.	53.	20.	0.27	0.4	0.24	1.6	0.6	1.32
E1	SD	90.	83.	4.	0.045	0.05	0.1	4.9	0.24	0.59
	MR	89.	84.	1.8	0.02	0.02	0.17	3.5	0.08	0.34

model, especially on large scales. On small scales the H_2 -regulated SF structures are affected by feedback due to a star formation more biased towards high density regions, which results in a more bursty star formation mode with large “bubbles” (like that seen in the centre of the panel of E1 model) forming more often.

3.5.1. *Non-equilibrium HI \leftrightarrow H₂ mass exchange*

For typical CNM HI densities the H_2 formation timescales are $\sim 5-50$ Myr (Eq. 4). The frothy gas disk structures evident in Figures 2 and 3 indicates the dynamic nature of the processes. In order to show this it is necessary to resolve the feedback effects in enough detail. Together with an assumed equilibrium f_m this will result in a more static picture for the ISM.

In figure 4 we demonstrate the non-equilibrium between the HI and H_2 gas phases by plotting the equilibrium f_m from section 2.2 as a function of density, and the actual non-equilibrium f_m from the simulations (for Z_\odot and $Z_\odot/5$). As we can see from this snapshot the gas is out of HI/ H_2 equilibrium for a large fraction of gas particles, with only the highest densities converging to equilibrium. The “ergodic” rather than particle-ensemble representation of this is demonstrated by the evolutionary track of a single gas particle in the $f_m - n$ plot (dashed line) showing that it spends most of the time away from equilibrium areas. This also means that both the collapse to higher densities and the destruction of H_2 in the diffuse gas phase is slow compared to the evolution of gas structures and ambient ISM conditions (further justifying the use of a time-dependent computation of f_m).

3.5.2. *The CO tracer molecule versus H₂*

The CO-rich H_2 distribution in Figures 2 and 3 is markedly different from the total H_2 distribution demonstrating a variable CO-to- H_2 mass ratio, especially for metal-poor systems. This can be seen more clearly in Figure 5, where we plot the pixel values drawn from the H_2 distribution against those drawn from the CO map. The values in figure 5 are scaled so that the maximum pixel values of the CO and the H_2 distributions match, which could be considered as an effective calibration of the CO-to- H_2 conversion factor for our simulations (observationally also performed at the bright end of CO-luminous H_2 clouds). It is clear that the CO-to- H_2 factor is not constant: the CO-rich H_2 distribution does show a tight correlation to the total H_2 mass distribution, but one that is much steeper than linear (and thus difficult to calibrate observationally without running into sensitivity limitations). This has been suspected and argued widely in the literature (Maloney and Black 1988; Pak et al. 1998, e.g.), so it is interesting that in our simple model this is demonstrated in the context of evolving galaxy models. Note that although a steeper CO- H_2 relation seems to appear for metal-rich compared to the metal-poor systems for the SD simulations (contrary to what would be expected for stationary cloud/radiation field models, e.g. Maloney and Black 1988; Pak et al. 1998), this trend disappears in the more realistic MR models.

The non-linear relation between CO and H_2 may also raise the possibility that (especially metal poor) galaxies can be “CO-dark” during certain epochs of their evolution (e.g. immediately after a burst of star

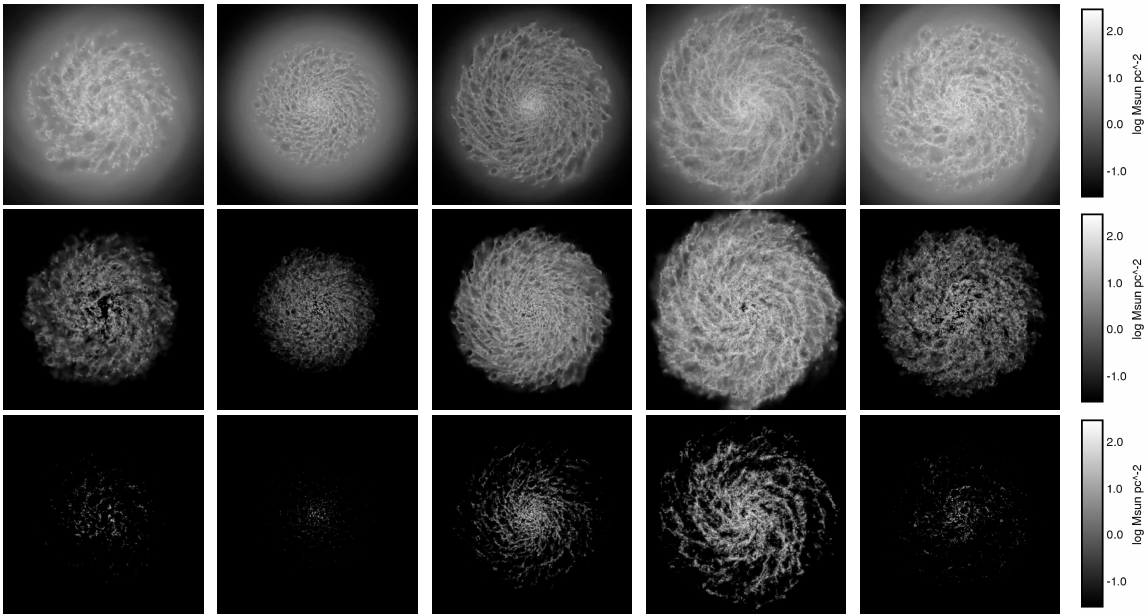


Fig. 2.— Gas distribution of simulations. Shown are (from top to bottom) HI distribution, the H₂ distribution and the CO map for runs (from left to right) A1-E1 after 1 Gyr of evolution and SD star formation. The A1 panels are 6 kpc across, the others 12 kpc.

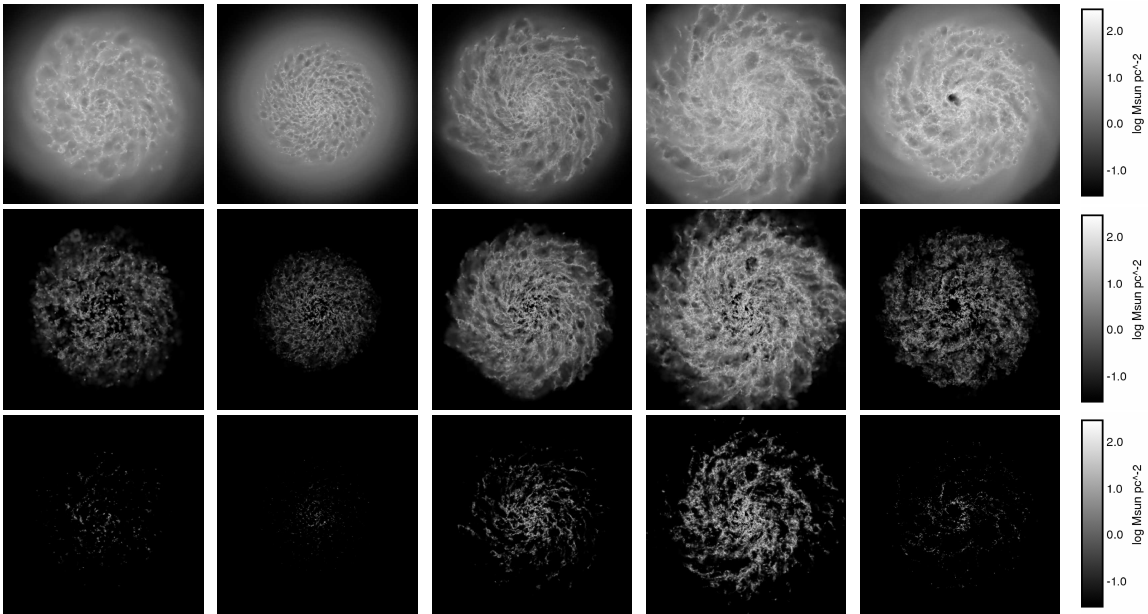


Fig. 3.— Gas distribution of simulations. Shown are (from top to bottom) HI distribution, the H₂ distribution and the CO map for runs (from left to right) A1-E1 after 1 Gyr of evolution and MR star formation.

formation and the subsequent enhancement of far-UV radiation), while H_2 gas is still there continuing forming stars. Such systems may appear as having much larger than usual star formation efficiencies, i.e. forming stars out of seemingly very little CO-bright H_2 gas. (we return to to this point in section 3.5.3 and 4).

Even strongly varying CO-to- H_2 relations can be difficult to discern and calibrate observationally. Direct methods would entail independent observations of CO *and* H_2 at comparable resolutions, an improbable proposition given that direct H_2 observations are difficult and thus rare. The latter are: a) observations of its lowest excitation S(0) line (Valentijn and van der Werf 1999, e.g.) which can be excited for CO-deficient H_2 (Papadopoulos et al. 2002), b) H_2 absorption studies in the far-UV. The S(0) line emission observations at $28\mu\text{m}$ are restricted to Space, where the small apertures deployed until now cannot match the resolution or gas-mass sensitivity attainable with ground-based CO observations using mm/sub-mm telescopes. Line absorption studies on the other hand are restricted by nature to single and special lines of sight, making routine comparisons with CO observations difficult especially for extragalactic environments. Krumholz et al. (2009) find considerably more H_2 detected by far-UV absorption studies with *FUSE* at low column densities than their CO, H_2 equilibrium model predicts, indicating that a CO-deficient diffuse H_2 phase is indeed present in the Galaxy. An indirect, but nevertheless powerful method relies on CO and C^+ observations at $158\mu\text{m}$ where any “excess” C^+ emission, after correcting for contributions from H^+ and WNM, CNM HI gas phases, is attributed to H_2 . Such observations have indicated $\sim 10-100$ times more H_2 gas than what CO emission reveals in the metal-poor and far-UV intense environment of the dwarf irregular IC 10 (Madden et al. 1997). These are indeed the type of environments where the largest disparities between H_2 and CO-rich H_2 distributions are expected from static (e.g. Bolatto et al. 1999) as well as our own dynamic models (see Figures 2, 3). Nevertheless C^+ observations still suffer from similar limitations like those of the S(0) line with the aforementioned example being one of the very few cases of meaningful comparisons with CO observations. Finally, with the CO-rich regions restricted deeper and deeper into H_2 clouds as metallicities decrease (Figures 2, 3) a rising “overpressure” on these regions is expected by the overlying CO-deficient H_2 gas. Such an effect has been recently detected (Bolatto et al. 2008).

3.5.3. *The K-S empirical relation*

Past investigations of the K-S empirical relations in galaxies used only stationary models (Dopita and Ryder 1994; Robertson and Kravtsov 2008). Testing for the emergence of robust K-S relations using dynamic galaxy models like ours could thus be very interesting, especially when the much more realistic H_2 -regulated star formation recipe is implemented. The relations between the gas mass surface densities (total, HI, H_2 and CO-rich H_2) and the local star formation density in our simulations are shown in Figures 6 (the SD model) and 7 (the MR model) (the CO surface density is normalized as in Figure 5). In each case the K-S relation as expressed in Kennicutt (1998) is also shown.

The first notable characteristic is that the K-S relation for the total gas or the HI surface density is closer to the observationally derived one for all the systems simulated here, both in terms of normalization

and slope. The slopes are generally between $n \approx 1.4$ and $n \approx 2$. In addition, the K-S relations for the CO-rich H_2 gas (tracing the densest molecular phase present in our simulations) have a more shallow slope ($n \approx 1-1.4$). This tendency of the K-S relation towards more linear slopes as one progresses from HI to CO-bright and then HCN-bright H_2 ($n \gtrsim 10^5 \text{ cm}^{-3}$) gas has also been noted observationally (Wong and Blitz 2002; Gao and Solomon 2004). The CO molecule will form in the highest density peaks of the H_2 distribution where short dynamical scales make them most intimately linked to the star formation.

There is some remaining uncertainty in the normalization of our derived empirical K-S relations when it comes to those involving the CO-rich H_2 gas (and thus directly comparable to observations). This is because far-UV absorption from the intervening dusty ISM (besides that in the natal clouds we considered here) will affect CO much more than the self-shielding H_2 through the galaxy, making the CO-rich H_2 distribution more extended than depicted in our models. This is expected to “shift” all our derived K-S relations involving CO to the right, but it is unlikely to reduce significantly the large deviations we find for the K-S relation in our simulated metal-poor systems ($Z = 0.2Z_\odot$) where far-UV is much less absorbed in their intervening ISM (i.e. between molecular clouds). In such systems the corresponding K-S relation is shifted upwards by a factor of $\sim 5-10$ with respect to the metal-rich ones (Fig 6, 7), yielding *a much more efficient star formation per CO-rich H_2 mass*. This is because in metal-poor systems H_2 and CO can form only in much denser gas (where star formation is most efficient) deeper in the CNM clouds, where higher densities make up for the loss of dust surface for H_2 and eventually CO formation. A similar effect was noted in metal poor dwarf galaxy IC10 (Leroy et al. 2006).

It is notable that the high gas fraction models (D1 and E1) have a somewhat *lower* SFR, i.e. their star formation rate per unit surface at a given surface density in these systems is lower, although the difference is not large ($< 50\%$). This is likely due to the fact that between two systems with similar total surface densities, the gas-rich one would necessarily have a smaller stellar component constraining the gas in the z-direction than the gas-poor one, resulting to less star formation per total surface density. Such effects have been described in the past, using K-S relations that involve the gaseous as well as the stellar mass component (Dopita and Ryder 1994). Finally, the MR models show a slight upward shift of all the K-S relations, but otherwise similar behaviour, despite the fact that the star formation is formulated in terms of the local molecular gas fraction. A K-S like law is known to arise under a wide set of conditions when the star formation rate scales with the reciprocal of the dynamical timescale $1/\sqrt{4\pi G\rho}$ (Schaye and Dalla Vecchia 2008). However the MR model inserts an additional non-trivial criterion (the H_2 richness of the star forming gas), and thus there is no reason for expecting so similar results (we return to this point in the Discussion).

3.5.4. The H_2 -pressure relation

In Figure 8 we show the H_2 -pressure relation for models A1-E1, where the average R_m is plotted versus midplane pressure P_{ext} , as estimated by Blitz and Rosolowsky (2006) (their equation 5),

$$P_{\text{ext}} = 272 \text{ cm}^{-3} \text{ K} \left(\frac{\Sigma_g}{\text{M}_\odot \text{ pc}^{-2}} \right) \left(\frac{\Sigma_\star}{\text{M}_\odot \text{ pc}^{-2}} \right)^{0.5}$$

$$\times \left(\frac{\sigma}{\text{km s}^{-1}} \right) \left(\frac{h_*}{\text{pc}} \right)^{-0.5}. \quad (19)$$

The velocity dispersion σ and the stellar scale height h_* are taken to be constants (as in Blitz and Rosolowsky 2006), while the gas surface density and stellar surface density are derived from the projected gas and stellar distributions. The R_m plotted is derived either from H_2 or the CO-rich H_2 surface density. As discussed previously the CO-rich H_2 surface density has an uncertainty in the absolute scaling, translating in some arbitrariness in the vertical scaling of the corresponding R_m - P_{ext} relation, but the trend of the R_m dependence on P_{ext} is not affected by this. Compared with the equilibrium H_2 -pressure relation of Figure 1 the plots here are more comparable to the actual observed quantities, given that the pressure used is the same indirect pressure estimate used in observations.

In Figure 8a-d a pressure dependence much flatter than the observed H_2 -pressure relation is found. For solar metallicity the trend with pressure is very flat while at lower metallicity it is steeper, but still short of a $n = 0.92$ slope derived by Blitz and Rosolowsky (2006). On the other hand, the relation derived for the CO-bright H_2 mass fraction R_{CO} has a steeper dependence and is very close to the observed slope for Z_\odot , while somewhat steeper for the $Z_\odot/5$ simulations. From what we have seen in figure 5, this is to be expected: this difference between H_2 and CO-rich H_2 in the H_2 -pressure relation derives from the bias of CO to form at higher gas densities, and thus pressures. The steeper fall-off of the CO-rich H_2 mass at lower densities compared to that of H_2 translates to a steeper fall-off of R_{CO} at lower pressures.

Our results indicate that, like the K-S relation for the CO-rich H_2 phase, the CO-rich H_2 -pressure relation should show a strong dependence on metallicity, and for $Z = Z_\odot/5$ it is considerably steeper than the Blitz and Rosolowsky (2006) relation. Although hampered by the very small number of actual CO detections at low metallicities, the available data suggest no strong trends with metallicity (Blitz and Rosolowsky 2006). Although some shift downwards is expected (Krumholz et al. 2009), the slope should be similar. For example, the IC 10 data points shown by Blitz and Rosolowsky (2006) lie very close to the normal relation. It will be interesting to see whether this will be borne out by further examination of low metallicity dwarf galaxies. In this context it is worth pointing out that the pressure estimate, based on the equation. 19 may not be valid for such systems due to their low stellar surface densities.

4. Discussion

Our numerical models suggest that after a dynamic equilibrium sets in the differences between MR and SD star formation recipes shown by the simulations are small. This is not only apparent from the star formation rates and/or a cursory examination of the resulting gas morphologies - which are determined mostly through feedback processes - but also borne out by the quantitative aspects of the SF behavior as revealed by the emergent K-S and B-R relations in our models. For the star formation process, within the range of SFRs explored in our simulations, the following picture then emerges: for diffuse gas to transform into star-forming gas it must evolve to higher densities and the conversion into H_2 proceeds passively at a certain high density threshold (set by formation rate and metallicity). In other words: star formation is

biased towards the higher densities where H_2 will form fast, and this becomes even more pronounced in low Z cases. However in the MR star formation model the phase converted to molecular gas has a star formation rate sufficiently slow so that its conversion into molecular gas is not the SF bottleneck (and thus star formation will not be affected, even in the cases where H_2 formation proceeds slowly).

We have demonstrated that robust phenomenological relations linking gas content to star formation (K-S relation), and molecular gas fraction (the SF fuel) to ambient ISM pressure (B-R relation), akin to those found in the local Universe, emerge out of realistic settings of dynamically evolving galaxy-sized systems of gas and stars. However, before considering the hereby presented investigation as validating the widespread practice of using K-S type of relations or SD star formation models as sub-grid physics in large scale galaxy evolution and cosmological models, we must point out that a considerable fraction of the current stellar mass has been assembled in major ULIRG type mergers (Smail et al. 1997; Hughes et al. 1998). In such systems destruction of H_2 can have much shorter timescales, induced by faster variations of the ambient far-UV field expected in starbursts (Parravano et al. 2003) yet also competing against a faster H_2 formation in their high density ISM gas. In such settings large deviations from (K-S)-type relations could occur, given that the latter seem to robustly emerge only after a dynamic equilibrium between HI, H_2 gas phases and stars has been established. Finally, in most numerical models the sub-grid K-S relation is set to use a much warmer gas phase ($\sim 10^3 - 10^4$ K) thermodynamically far removed from the CNM HI and the H_2 gas that are directly linked to star formation.

Modelling of ULIRG type systems is computationally more challenging as the high temperatures at high densities mean that timestepping of the simulation will be slower and the implicit assumptions that we make about the transparency of the interstellar medium break down as the star formation sites in these are obscured on galactic scales, so at the moment directly testing this is not possible. However, as an instructive first step to examine the validity of the K-S relation during the early evolution of galaxies, we can examine our galaxy models during the early phases of the simulation, when the ISM phases and star formation have yet to establish a dynamical equilibrium. This is shown in in Figure 9, from which it can readily be discerned that at early evolutionary timescales significant deviations of the star formation from that expected from the K-S relation do occur, and are especially pronounced for metal-poor systems (A1, B1, and E1). In the latter cases there are periods when the CO-derived K-S relation will overestimate or underestimate the underlying star formation which, for gas-rich *and* metal-poor systems (E1), can last well into later evolution times ($T \sim 0.2 - 0.5$ Gyrs). This seems to be an effect of the greater sensitivity of CO destruction at low metallicities where this molecule survives only in the densest of the CNM gas, itself spawning star-forming regions very fast, which in turn destroy CO. The fact that this behavior emerges for both a small (A1) and a $10\times$ larger metal-poor system (B1) suggests that this “oscillating” of the SFR with respect to a K-S(CO) relation (Figure 9) is not due to large stochastic scatter from a smaller number of star forming sites. On the other hand the CO-derived K-S relation seems to remain a good predictor of the underlying star formation, even at early evolutionary times, for metal-rich systems with moderate amounts of gas (C1, C1-MR), i.e. like those used for its establishment in the local Universe.

The largest deviations between the SFR predicted from the K-S relation and the actual one occur for the K-S(HI+ H_2) and K-S(H_2) relations during early evolutionary times ($T \lesssim 0.2 - 0.3$ Gyrs), and are particularly

pronounced for the very gas-rich systems (Fig.9: E1, D1 models). In these cases even the K-S(CO) relation underpredicts the true SFR, even for the metal-rich system (D1) where CO tracks H_2 well, and thus cannot be due to CO failing to trace H_2 (the SF fuel) well. During those early epochs gas-rich systems can appear as undergoing periods of very efficient star formation (i.e. little CO-bright H_2 gas but lots of ongoing star formation), where application of the K-S(CO) relation using their observed SFRs would imply much more molecular gas than there is. Such systems, though more massive than those modeled here, may have been recently observed at high redshifts (Tacconi et al. 2008).

The failure of the standard K-S($HI+H_2$) relation to track SFRs during the early evolution of very gas-rich systems is rather expected given that this relation is “blind” to the thermodynamic state of the gas, and thus can equally well make stars out of $10^4 K$ WNM HI or $30 K$ H_2 gas. Only at later times its SFR predictions become valid, result of a dynamic equilibrium among the various ISM phases and the stellar component being established. This could have implications for modelling of the gas-rich galaxies found in the distant Universe, or systems where major gas mass accretion events “reset” their evolutionary states back to gas-rich ones. In such cases the non-equilibrium, non-linear, mass/energy exchange between the various ISM phases and the stellar component may come to dominate significant periods of intense star formation and stellar mass built-up during which not even the most realistic, CO-derived, K-S relation seems applicable (Figure 9: models E1, D1).

5. Conclusions

We use our time-varying, galaxy-sized, numerical models of gas+stars that track the ISM thermodynamics and the $HI \leftrightarrow H_2$ gas phase exchange, to investigate: a) the emergence of two prominent empirical relations deduced for galaxies in the local Universe: the Kennicutt-Schmidt (K-S) relation and the H_2 -pressure relation, b) the effects of a more realistic H_2 -regulated star formation recipe, and c) the evolution of very gas-rich systems. Our models now include a separate treatment for formation and destruction of the H_2 -tracing CO molecule, which allows a direct comparison of such models with observations, and a new independent investigation of the CO- H_2 concomitance in the ISM of evolving galaxies. Our findings can be summarized as follows

- For ISM states of H_2/HI equilibrium, an H_2 -pressure relation close to the one observed robustly emerges for a wide range of parameters, with a strong dependence mostly on metallicity. For the more realistic non-equilibrium H_2/HI states *only the CO-bright H_2 phase shows an H_2 -pressure relation similar to the one observed.*
- The H_2 -regulated star formation model successfully models star formation without the adhoc parameter of the local star formation efficiency adopted by most galaxy-sized numerical models, while incorporating a fundamental aspect of the star formation process.
- A comparison between numerical models using the usual simple-delay (SD) and the new molecular-regulated (MR) star formation recipes reveals very few differences. It shows a factor of $\sim 3-4$ more

efficient star formation per CNM gas mass than the case of MR star formation.

- We find little sensitivity of the global SF efficiency $M(\text{HI}+\text{H}_2)/\text{SFR}$ to the SF recipe chosen, once dynamic equilibrium between ISM phases and stars is established, yielding confidence to (K-S)-type of relations emerging as a general characteristic of galaxies.
- A non-equilibrium $\text{HI} \leftrightarrow \text{H}_2$ gas mass exchange is revealed taking place under typical ISM conditions, demonstrating the need for a full dynamic rather than stationary treatment of these ISM phases.
- The CO molecule can be a poor, non-linear, tracer of the true underlying H_2 gas distribution, especially in metal-poor systems, and even in those with very high gas mass fractions (more typically found at high redshifts).
- A K-S relation robustly emerges from our time-dependent models, irrespective of the SF recipe used, after a dynamical equilibrium is established ($T \gtrsim 1$ Gyr). The CO-derived K-S relation has a more shallow slope than the one involving the total gas mass, and as in the H_2 -pressure relation, a strong dependence on metallicity is found.
- At early evolutionary timescales ($T \lesssim 0.4$ Gyr) our models show *significant and systematic deviations of the true star formation from that expected from the K-S relation*, which seem especially pronounced and prolonged for metal-poor systems. These deviations occur even for the CO-derived K-S relation (the more realistic one since CO is directly observable and traces the densest H_2 gas which “fuels” star formation), and even for metal-rich systems where CO tracks the H_2 gas well.
- The largest deviations from the K-S relation occur at the earliest evolutionary stages of the systems modeled here ($T \lesssim 0.2$ Gyr) and for the most gas-rich ones. During this time significantly higher star formation rates per CO-bright H_2 gas mass occur, and such star-forming galaxies may have been already observed at high redshifts.

Finally we must note that when it comes to the gas-rich galaxies accessible to current observational capabilities at high redshifts, our results, drawn for much less massive systems, remain provisional. Nevertheless for more massive gas-rich systems the larger amplitudes of ISM equilibrium-perturbing agents (e.g. SNs, far-UV radiation fields), and the shorter timescales that will characterize their variations are more likely than not to exaggerate the deviations of true star formation versus the one derived from (K-S)-type phenomenological relations. A dedicated observational effort to study such galaxies at high redshifts (soon to be dramatically enhanced by ALMA), as well as extending detailed numerical modeling of gas and stars to larger systems (as computational capabilities improve), can help establish whether (K-S)-type relations remain valid during most of the stellar mass built-up in galaxies, or only emerge after dynamic equilibrium has been reached during much latter evolutionary stages.

REFERENCES

Barnes, J. & Hut, P., 1986, *Nature* **324**, 446

- Blitz, L., 1997, in W. B. Latter, S. J. E. Radford, P. R. Jewell, J. G. Mangum, & J. Bally (eds.), *IAU Symposium*, Vol. 170 of *IAU Symposium*, pp 11–18
- Blitz, L. & Rosolowsky, E., 2004, *ApJ* **612**, L29
- Blitz, L. & Rosolowsky, E., 2006, *ApJ* **650**, 933
- Bolatto, A. D., Jackson, J. M., & Ingalls, J. G., 1999, *ApJ* **513**, 275
- Bolatto, A. D., Leroy, A. K., Rosolowsky, E., Walter, F., & Blitz, L., 2008, *ArXiv e-prints* 807
- Bruzual A., G. & Charlot, S., 1993, *ApJ* **405**, 538
- Buch, V. & Zhang, Q., 1991, *ApJ* **379**, 647
- Dickman, R. L., Snell, R. L., & Schloerb, F. P., 1986, *ApJ* **309**, 326
- Dobbs, C. L., Bonnell, I. A., & Pringle, J. E., 2006, *MNRAS* **371**, 1663
- Dopita, M. A. & Ryder, S. D., 1994, *ApJ* **430**, 163
- Draine, B. T., 1978, *ApJS* **36**, 595
- Elmegreen, B. G., 1989, *ApJ* **338**, 178
- Elmegreen, B. G., 1993, *ApJ* **411**, 170
- Elmegreen, B. G., 2000, *ApJ* **530**, 277
- Elmegreen, B. G., 2002, *ApJ* **577**, 206
- Federman, S. R., Glassgold, A. E., & Kwan, J., 1979, *ApJ* **227**, 466
- Gao, Y. & Solomon, P. M., 2004, *ApJ* **606**, 271
- Garnett, D. R., 1998, in D. Friedli, M. Edmunds, C. Robert, & L. Drissen (eds.), *Abundance Profiles: Diagnostic Tools for Galaxy History*, Vol. 147 of *Astronomical Society of the Pacific Conference Series*, pp 78–+
- Gerritsen, J. P. E., 1997, *Ph.D. thesis*, , Groningen University, the Netherlands, (1997)
- Glover, S. C. O. & Mac Low, M.-M., 2007, *ApJS* **169**, 239
- Goldshmidt, O. & Sternberg, A., 1995, *ApJ* **439**, 256
- Henry, R. B. C., 1998, in D. Friedli, M. Edmunds, C. Robert, & L. Drissen (eds.), *Abundance Profiles: Diagnostic Tools for Galaxy History*, Vol. 147 of *Astronomical Society of the Pacific Conference Series*, pp 59–+
- Heyer, M. H. & Brunt, C. M., 2004, *ApJ* **615**, L45

- Hidaka, M. & Sofue, Y., 2002, *PASJ* **54**, 223
- Honma, M., Sofue, Y., & Arimoto, N., 1995, *A&A* **304**, 1
- Hughes, D. H., Serjeant, S., Dunlop, J., Rowan-Robinson, M., Blain, A., Mann, R. G., Ivison, R., Peacock, J., Efstathiou, A., Gear, W., Oliver, S., Lawrence, A., Longair, M., Goldschmidt, P., & Jenness, T., 1998, *Nature* **394**, 241
- Israel, F. P., 1997, *A&A* **328**, 471
- Jura, M., 1974, *ApJ* **191**, 375
- Katz, N., 1992, *ApJ* **391**, 502
- Kennicutt, Jr., R. C., 1989, *ApJ* **344**, 685
- Kennicutt, Jr., R. C., 1998, *ApJ* **498**, 541
- Kobayashi, N., Yasui, C., Tokunaga, A. T., & Saito, M., 2008, *ApJ* **683**, 178
- Krumholz, M. R., McKee, C. F., & Tumlinson, J., 2009, *ApJ* **693**, 216
- Larson, R. B., 1981, *MNRAS* **194**, 809
- Leroy, A., Bolatto, A., Walter, F., & Blitz, L., 2006, *ApJ* **643**, 825
- Madden, S. C., Poglitsch, A., Geis, N., Stacey, G. J., & Townes, C. H., 1997, *ApJ* **483**, 200
- Maloney, P. & Black, J. H., 1988, *ApJ* **325**, 389
- Martin, P. G., Keogh, W. J., & Mandy, M. E., 1998, *ApJ* **499**, 793
- Mo, H. J., Mao, S., & White, S. D. M., 1998, *MNRAS* **295**, 319
- Monaghan, J. J., 1992, *ARA&A* **30**, 543
- Navarro, J. F. & White, S. D. M., 1993, *MNRAS* **265**, 271
- Omont, A., 2007, *Reports of Progress in Physics* **70**, 1099
- Pak, S., Jaffe, D. T., van Dishoeck, E. F., Johansson, L. E. B., & Booth, R. S., 1998, *ApJ* **498**, 735
- Papadopoulos, P. P., Thi, W.-F., & Viti, S., 2002, *ApJ* **579**, 270
- Papadopoulos, P. P., Thi, W.-F., & Viti, S., 2004, *MNRAS* **351**, 147
- Parravano, A., Hollenbach, D. J., & McKee, C. F., 2003, *ApJ* **584**, 797
- Pelupessy, F. I., 2005, *Ph.D. thesis*, Leiden Observatory, Leiden University, P.O. Box 9513, 2300 RA Leiden, The Netherlands

- Pelupessy, F. I., Papadopoulos, P. P., & van der Werf, P., 2006, *ApJ* **645**, 1024
- Pelupessy, F. I., van der Werf, P. P., & Icke, V., 2004, *A&A* **422**, 55
- Rana, N. C. & Wilkinson, D. A., 1986, *MNRAS* **218**, 721
- Robertson, B. E. & Kravtsov, A. V., 2008, *ApJ* **680**, 1083
- Röllig, M., Ossenkopf, V., Jeyakumar, S., Stutzki, J., & Sternberg, A., 2006, *A&A* **451**, 917
- Savage, B. D., Bohlin, R. C., Drake, J. F., & Budich, W., 1977, *ApJ* **216**, 291
- Schaye, J. & Dalla Vecchia, C., 2008, *MNRAS* **383**, 1210
- Semelin, B. & Combes, F., 2002, *A&A* **388**, 826
- Smail, I., Ivison, R. J., & Blain, A. W., 1997, *ApJ* **490**, L5+
- Solomon, P. M., Rivolo, A. R., Barrett, J., & Yahil, A., 1987, *ApJ* **319**, 730
- Solomon, P. M. & Vanden Bout, P. A., 2005, *ARA&A* **43**, 677
- Spitzer, Jr., L. & Jenkins, E. B., 1975, *ARA&A* **13**, 133
- Springel, V., Di Matteo, T., & Hernquist, L., 2005, *MNRAS* **361**, 776
- Springel, V. & Hernquist, L., 2002, *MNRAS* **333**, 649
- Steidel, C. C., Adelberger, K. L., Giavalisco, M., Dickinson, M., & Pettini, M., 1999, *ApJ* **519**, 1
- Tacconi, L. J., Genzel, R., Smail, I., Neri, R., Chapman, S. C., Ivison, R. J., Blain, A., Cox, P., Omont, A., Bertoldi, F., Greve, T., Förster Schreiber, N. M., Genel, S., Lutz, D., Swinbank, A. M., Shapley, A. E., Erb, D. K., Cimatti, A., Daddi, E., & Baker, A. J., 2008, *ApJ* **680**, 246
- Valentijn, E. A. & van der Werf, P. P., 1999, *ApJ* **522**, L29
- Walter, F., Bertoldi, F., Carilli, C., Cox, P., Lo, K. Y., Neri, R., Fan, X., Omont, A., Strauss, M. A., & Menten, K. M., 2003, *Nature* **424**, 406
- Wolfire, M. G., Hollenbach, D., McKee, C. F., Tielens, A. G. G. M., & Bakes, E. L. O., 1995, *ApJ* **443**, 152
- Wolfire, M. G., McKee, C. F., Hollenbach, D., & Tielens, A. G. G. M., 2003, *ApJ* **587**, 278
- Wong, T. & Blitz, L., 2002, *ApJ* **569**, 157
- Zuckerman, B. & Evans, II, N. J., 1974, *ApJ* **192**, L149

Fig. 4.— Equilibrium and non-equilibrium f_m values versus gas density. The equilibrium f_m of particles in the simulation (diamonds) and the non-equilibrium f_m (dots) as a function of density for $Z = \odot/5$ (left panel) and $Z = Z_\odot$ (right panel). The equilibrium f_m is calculated from the instantaneous particle properties. The dashed line marks a time track of a typical gas particle experiencing a cycle of collapse, star formation and reheating, with square symbols placed at 0.93 Myr intervals.

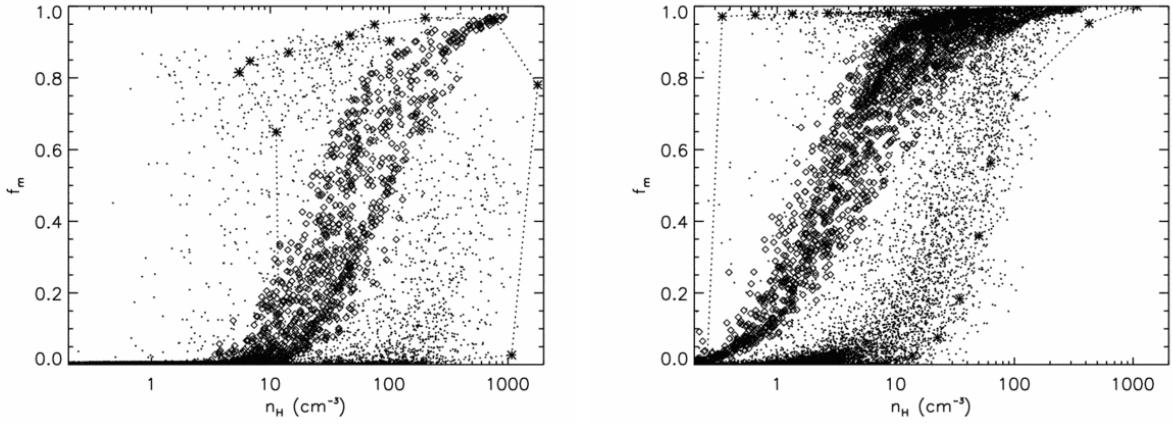


Fig. 5.— H_2 versus CO-rich H_2 mass surface density. Plotted are the pixel values of the projections of the gas distribution for the SD SF model for low (left upper panel) and solar (right upper panel) metallicities (models B1 and C1). Lower left and Lower right panels show the corresponding results for the MR SF recipe. The CO pixel values are normalized as described in the text. For reference a long dashed line with linear slope ($n = 1$) is plotted, as well as a short dashed line with a slope $n = 2$.

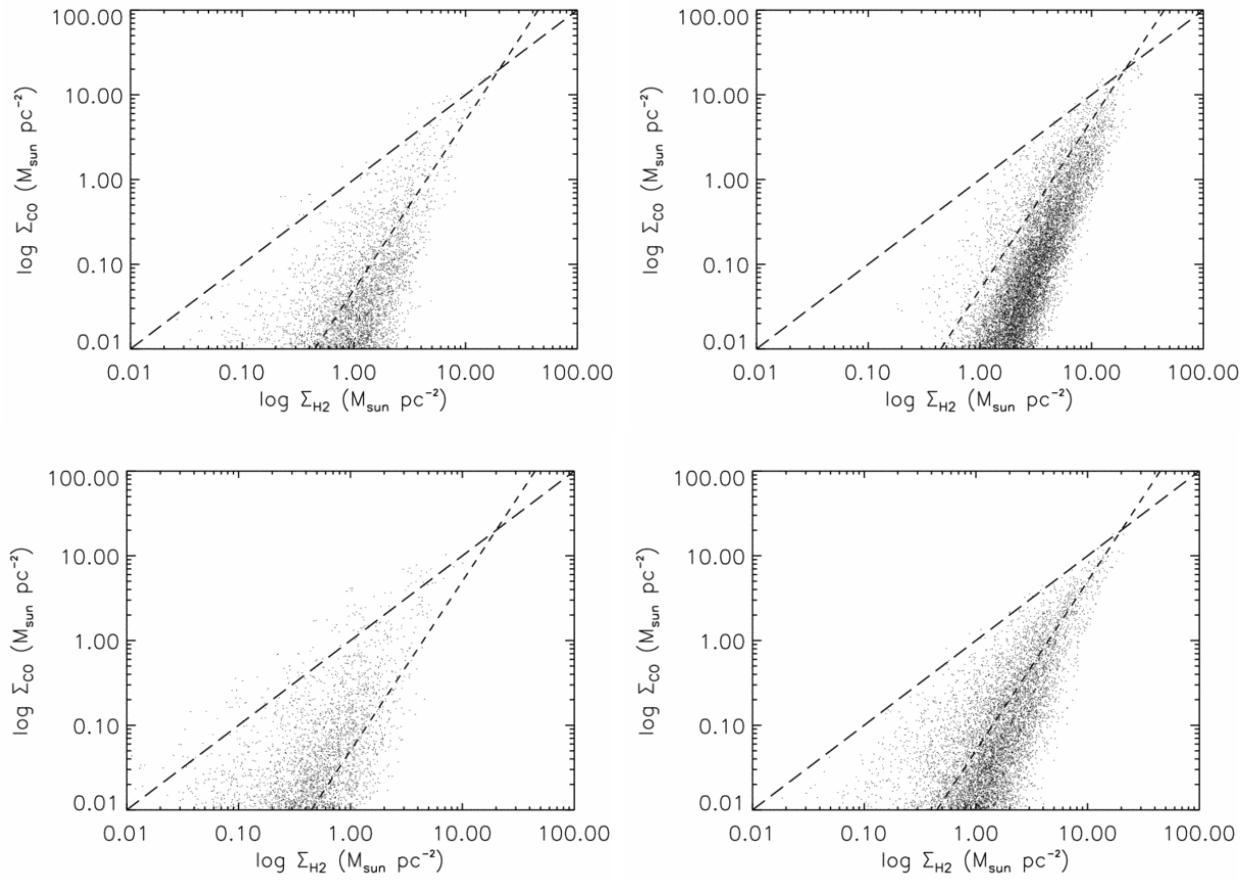


Fig. 6.— Kennicutt-Schmidt laws: The star formation density for the simulations A1-E1 (from top row to bottom row) using the SD star formation recipe vs (panels from left to right) the total, the neutral, H_2 or CO-rich H_2 gas surface density. Shown are mean relations (points are averaged in equal logarithmic bins of surface density). The short dashed line shows the empirical Kennicutt (1998) relation with a slope of $n = 1.4$ as a reference, whereas the long dashed and dotted lines have of $n = 2$ and $n = 1$ respectively. Note that some outliers are probably affected by image artefacts from the projection of the star particles.

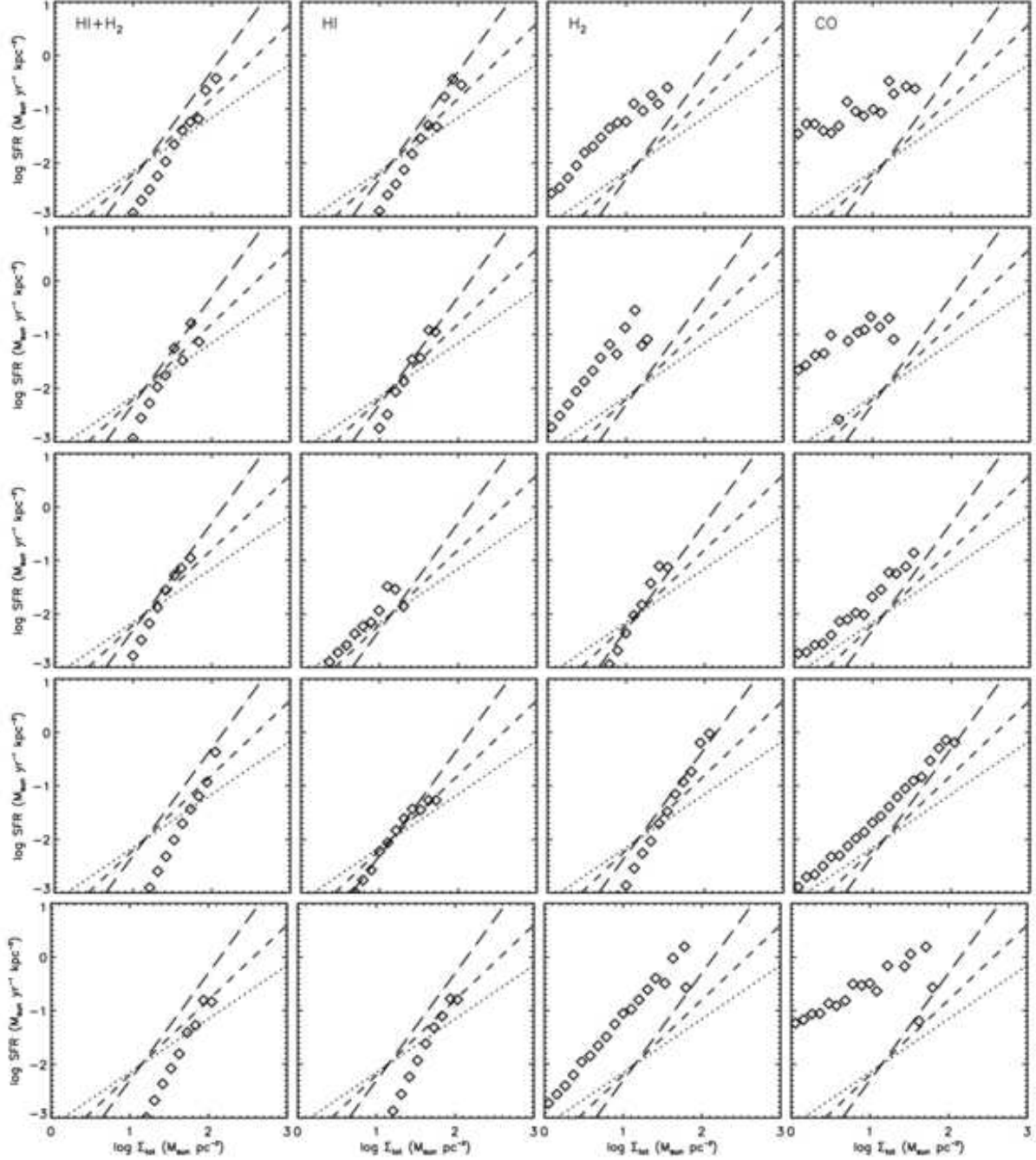
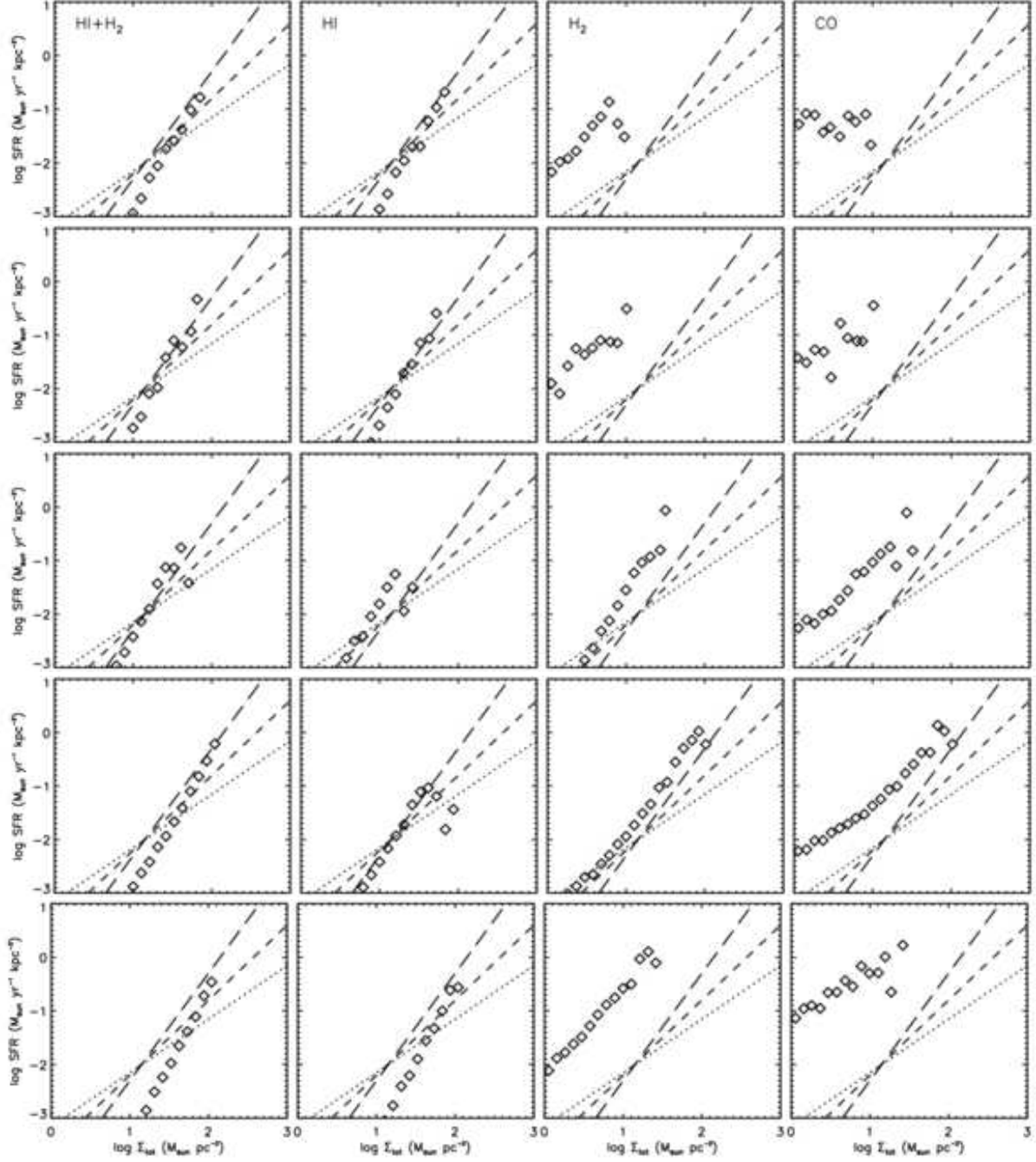


Fig. 7.— Kennicutt Schmidt laws. Same as figure 6, but for the MR star formation recipe.



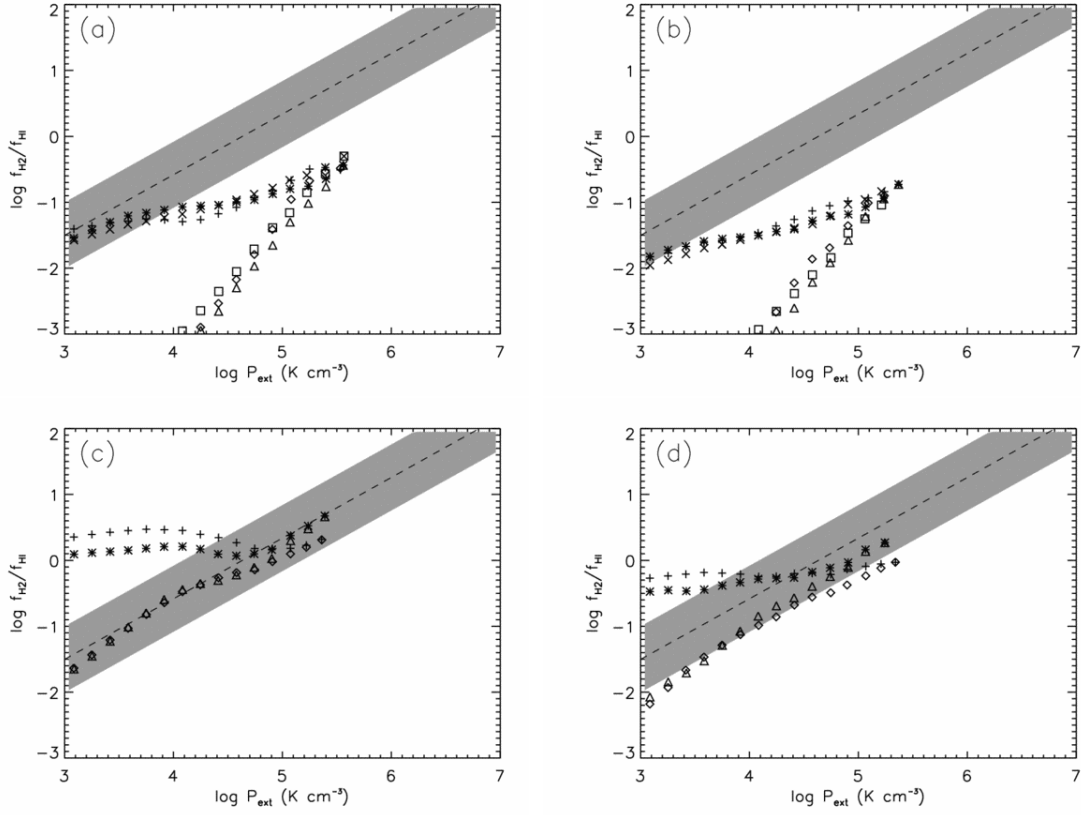


Fig. 8.— Simulation results for $R_m = f_{\text{H}_2}/f_{\text{HI}}$. Panels show $R-m$ as a function of midplane pressure for the low metallicity models (A1,B1 and E1) for the SD star formation model (panel a) and the MR model (b) and for solar metallicity models (C1 and D1) with the SD model (c) and MR model (d). The star like symbols indicate that R_m is estimated from the H_2 maps, while open symbols indicate that CO is used.

Fig. 9.— Time dependence of the SFR versus that expected from the K-S relation and the instantaneous gas content. Shown are the actual total star formation (drawn black line) taking place in the models A1, B1, C1 for SD or MR star formation recipe (indicated in the lower right of each panel). All other lines give the SFRs expected from various applications of the K-S relation (with slope $n=1.4$) using: total gas surface density (dashed), H_2 gas surface density (dash-dotted), and CO-bright H_2 gas surface density (dotted). The KS star formation lines are normalized such that their average after 300 Myr matches the average star formation over the same period.

